Matter and Radiation at Extremes | RESEARCH ARTICLE | pubs.aip.org/aip/mre

Shock standards Cu, Ag, Ir, and Pt in a wide pressure range

Cite as: Matter Radiat. Extremes 8, 046901 (2023); doi: 10.1063/5.0124555
Submitted: 6 September 2022 • Accepted: 18 April 2023 •
Published Online: 16 May 2023

Leonid Burakovsky,[a] Dean L. Preston, Scott D. Ramsey, Charles E. Starrett, and Roy S. Baty

AFFILIATIONS

Los Alamos National Laboratory, Los Alamos, New Mexico 87545, USA

[a]Author to whom correspondence should be addressed: burakov@lanl.gov

ABSTRACT

Although they are polymorphic (multiphase) materials, both copper and silver are reliable Hugoniot standards, and thus it is necessary to establish an accurate analytic model of their principal Hugoniots. Here we present analytic forms of their principal Hugoniots, as well as those of iridium and platinum, two "pusher" standards for shock-ramp experiments, over a wide range of pressures. They are based on our new analytic model of the principal Hugoniot [Burakovsky *et al.*, J. Appl. Phys. **132**, 215109 (2022)]. Comparison of the four Hugoniots with experimental and independent theoretical data (such data exist to very high pressures for both copper and silver) demonstrates excellent agreement. Hence, the new model for copper and silver can be considered as providing the corresponding Hugoniot standards over a wide pressure range. We also suggest an approach for calculating the Grüneisen parameter along the Hugoniot and apply it to copper as a prototype, and our results appear to be in good agreement with the available data.

I. INTRODUCTION

In modern static devices [diamond anvil cells (DACs)], samples can be pressurized to a few megabars. Shock-wave experiments allow higher pressures to be attained, for example, 5–10 Mbar in light-gas guns in a plane geometry. There are different schemes for such experiments. Among these, the so-called impedance-matching scheme clearly stands out. In this scheme, a uniform shock wave is initially generated in the standard, by an explosion, by a strike from an accelerated plate, or by laser-irradiation-induced ablation. Next, the shock wave penetrates the sample. The impedance-matching technique is reviewed in detail in Ref. 1. This technique is the most widely used, because a two-layer target consisting of a well-studied substance (a standard) and the sample under investigation is best suited for carrying out a large number of measurements.

In these experiments, the possibilities for obtaining the desired data are rather limited. The simplest and most reliable are measurements of shock velocities U_s in both substances. If the equation of state (EOS) of the standard is known, then it can be used along with the two known U_ss to calculate the particle velocity U_p in the sample. With these data, combined with the Rankine–Hugoniot relations, the density ρ of the sample, and the pressure P and internal energy E behind the shock front can be determined. If only the Hugoniot of the standard is known, then the U_p in the sample will be calculated approximately. The closer the dynamic rigidities of the sample and the standard, the more accurate will be the calculation of U_p and of ρ, P, and E. In any event, accurate knowledge of the Hugoniot of the standard is crucial: errors in the Hugoniot standard propagate as systematic errors in the inferred density and pressure in shock-wave experiments. This is particularly pertinent for highly compressible materials such as deuterium and helium.

In previous studies at Los Alamos, Al-24ST aluminum alloy and brass were used as the standards for investigating light and heavy substances, respectively.[2,3] In the USSR, iron was used as the standard.[4] The corresponding Hugoniots of these three metals were determined via the experimental scheme of colliding plates of the same material. However, none of these three metals represents a reliable Hugoniot standard. In iron, at 13.2 GPa, a phase transition from the body-centered cubic (bcc) α-Fe phase (which is the ambient solid phase of Fe) to the hexagonal close-packed (hcp) ε-Fe phase occurs on its principal Hugoniot (see Ref. 5 for a review), and the two structures have different EOS. A second phase transition, from ε-Fe to another solid phase of iron, prior to melting on the Hugoniot, may have been seen in experiments,[6,7] but to date its occurrence has been a subject of debate in the literature (see Ref. 8 for a review). In an experiment in which 4 Gbar, one of the highest

Hugoniot pressures reported in the literature so far, was achieved,[9] a material whose physical properties can be approximated well by those of iron, namely, type 20 steel with a density of 7.85 g/cm^3, was used as a Hugoniot standard. As claimed in Ref. 9, it was chosen because both the Hugoniot and isentropes of Fe deviate only slightly from the predictions of Thomas–Fermi-type models in the region of thermodynamic variables required for the analysis of the experimental data of Ref. 9. Thus, iron could serve as a Hugoniot standard, albeit at much higher pressures; at low and moderate pressures, iron is not suitable to be considered as a reliable Hugoniot standard. Similarly, neither aluminum nor brass are suitable as standards, because the phase diagram of Al contains three solid phases, fcc, hcp, and bcc,[10] with EOS quite different from each other, and there may be a fcc–bcc solid–solid phase transition along the Hugoniot.[11] Brass is rather elastic, which limits from below the pressures at which its Hugoniot standard can be considered as reliable.

Both copper and silver are free from the above disadvantages. They are plastic materials, and so their characteristics of shock-wave and static compression agree well with each other. Besides being ductile, copper, silver, and gold are the three most malleable metals of all. Both copper and silver are polymorphic materials, and each of them experiences an fcc–bcc solid–solid phase transition along the Hugoniot.[12,13] However, in both cases, the EOS of the fcc and bcc phases are very close to each other, and the volume change at the transition is very small, in view of the fact that the fcc–bcc solid–solid phase boundary is virtually flat in both cases,[12,13] and so the Clausius–Clapeyron relation $\Delta V/\Delta S = dT/dP \approx 0$ gives $\Delta V \approx 0$. Hence, both solid structures can be reliably described by a common EOS. Since the volume change at melting is also small, each of the two Hugoniots is virtually continuous across both the solid–solid phase transition and melting. Thus, either of the two substances represents a very reliable Hugoniot standard.

We note that wide use of the impedance-matching method described above requires the availability of several Hugoniot standards with different dynamic rigidities. Another two materials, namely, platinum and iridium, have been suggested both as Hugoniot standards and as "pusher" standards for modified shock-ramp experiments on the Z platform at Sandia National Laboratories (SNL).[14] The technique of modified shock-ramp experiments is similar to the impedance-matching one, since a pusher is inserted between an electrode (a flyer) and the sample such that the initial shock-ramp compression wave is generated in the pusher and then enters the sample.[15] Both Pt and Ir could be considered as "ideal" pusher materials because of their high acoustic impedances (to avoid re-shock reflection from the sample), low sound speeds to delay reverberation (being among the materials having the highest densities of all), and low degree of nonlinearity in compression to minimize steepening. However, they cannot be considered as reliable Hugoniot standards, because of the presence of a structural phase transition, namely, an fcc–randomly disordered hcp (rhcp) solid–solid one. This transition was theoretically predicted to occur in both Pt[16] and Ir,[17] and the most recent experimental studies seem to confirm its occurrence.[14,18] Specifically, an anomalous velocity dispersion is observed in Pt ramp-compressed from a ~85 GPa-shocked state on the driven side of the sample, at ~150 GPa and $T \sim 2000$–3000 K (according to the EOS), which are the P–T conditions of the rhcp phase.[16] This dispersion is real and reproducible: VISAR contrast decreases when it occurs, different velocities are observed in different (closely spaced) probes, and it is observed in both free-surface and windowed samples, at a velocity corresponding to the same driven-side pressure.[14] In Ir, a phase transition is detected in the shock-compression data at a particle velocity of ~1.3 km/s ($P \sim 170$ GPa) from piecewise fitting of the data,[18] which is consistent with the $P = 166.5$ GPa predicted theoretically for the fcc–rhcp transition on the Ir Hugoniot.[17]

Hence, only Cu and Ag remain as the most reliable candidates for Hugoniot standards. Hence, an accurate model of their principal Hugoniots is really necessary, and not only for the processing of the shock-wave data, but also for the ruby pressure scale, which we now dwell on in some more detail. The ruby pressure scale, in which P is measured on the basis of the R_1 line shift of ruby luminescence, is one of the most widely used pressure standards in DAC experiments. To date, the most popular calibration of this pressure scale has been that of Mao *et al.*,[19] who measured the R_1 line shift in an argon medium up to a pressure of 80 GPa while the pressure was determined from room-temperature isotherms of Cu and Ag calculated by Carter *et al.*[20] on the basis of the corresponding shock-wave data alone (without taking into account ultrasonic measurements). Since then, the range of shock-wave data on both Cu and Ag has been expanded significantly; for example, the experimental shock-wave data on Cu now extend up to as high as 20.4 TPa.[21] For Ag, the experimental shock-wave data are available to 300 GPa.[22] In what follows, we present a new analytic model for their principal Hugoniots that is applicable over a wide pressure range.

The use of Cu as an absolutely calibrated sound-velocity standard for high-precision measurements at pressures in excess of 400 GPa was advocated in Ref. 23, in which the results of absolute measurements of the Hugoniot and sound velocity of copper for pressures from 500 to 1200 GPa were presented. The shock Hugoniot of Cu was calculated theoretically in Ref. 24 for the purpose of using Cu as a shock standard. In the experiments reported in Ref. 9 and mentioned above, shock velocities of ~350 km/s, and accordingly pressures of ~7.5 Gbar (7.5×10^5 GPa), were achieved in the iron standard (and, respectively, ~450 km/s and ~4 Gbar in Al, whose Hugoniot was measured). Since the locations of Fe ($Z = 26$) and Cu ($Z = 29$) in the periodic table are close to each other, and since the basic mechanical and thermodynamic variables scale with atomic number Z (in particular, $P/Z^{10/3}$ is a function of ZV, where V is the molar volume),[25] future experiments on Cu should be expected to achieve shock velocities and pressures of similar magnitude. Since such shock velocities and pressures correspond to the Hugoniot turnaround point (discussed in what follows), it is essential to have available a reliable analytic model of the Cu Hugoniot over a very wide pressure range, including that of its turnaround point. The need for knowledge of the analytic form of the principal Hugoniot of Cu over a wide pressure range was also emphasized by Kalitkin and Kuz'mina.[26] The importance of a reliable analytic model of the principal Hugoniot in a general case that covers a pressure range extending well beyond that of the turnaround point is discussed in more detail in Sec. III.

We note that some other substances have been proposed as Hugoniot standards, such as molybdenum[27] and SiO_2, as both α-quartz[27–30] and fused silica, the amorphous form of SiO_2.[31] However, a detailed discussion of both the advantages and shortcomings of their use in shock-wave experiments goes beyond the scope of this work.

II. PRINCIPAL HUGONIOT OVER A WIDE PRESSURE RANGE

We will construct analytic models of the principal Hugoniots of the four shock standards, namely, two Hugoniot standards Cu and Ag, and two pusher standards Ir and Pt for modified shock-ramp experiments, using the analytic framework established in our previous publication.[32] In this framework, a wide P range is divided into three regimes, and the Hugoniot is constructed in each of these regimes and then interpolated smoothly between them. These regimes are (i) the low-P regime in which the Hugoniot is described by $U_s = C + BU_p$, where U_p and U_s are the particle and shock velocities, respectively, and the values of C and B come from experiment, (ii) the intermediate-P regime (discussed in more detail below) where the Hugoniot is described by the Thomas–Fermi–Kalitkin (TFK) model[33,34] $U_s = c + bU_p + aU_p^2$, with the values of c, b and a determined virtually for all Zs,[33–35] and (iii) the high-P regime in which the Hugoniot is described by the Debye–Hückel–Johnson (DHJ) model.[36–38] The only assumption that is made is that the principal Hugoniot is governed by some function $U_s = U_s(U_p)$ (which is linear at low P and quadratic at intermediate P; its high-P form was established in Ref. 32) and that this function is continuous and smooth (the first derivative dU_s/dU_p is continuous) at all U_p. Then it follows from the Rankine–Hugoniot relations[32] that compression ratio, pressure, and internal energy are all continuous and smooth as well. No other assumptions, and no additional free parameters except the six mentioned above, namely, C, B, c, b, a, and Z, are required for the construction of the analytic model of the principal Hugoniot. To match the next regime, the linear form of the low-P regime is modified to $U_s = C + BU_p + AU_p^2$, where A is an additional, seventh, parameter that introduces a very small nonlinearity ($A \sim 10^{-2}$ s/km) and is obtained using the formula $A = a - (B-b)^2/[4(c-C)]$.[32]

The names of the three P regimes of the principal Hugoniot may sound confusing and may not correspond to those adapted in high-pressure research in general and phase diagram and EOS studies in particular. Specifically, high-P is generally taken to mean pressures in excess of ~100 GPa. In our case, the low-P–med-P transition point corresponds to shock velocities of ~10 km/s (see, e.g., Table I); with ambient densities of ~1–10 g/cm^3, this corresponds to pressures of ~100–1000 GPa. Thus, our med-P regime is analogous to the more familiar high-P range of EOS studies. Our med-P–high-P transition point corresponds to $P \sim 1$–10 Gbar (10^5–10^6 GPa).

The following is a brief summary of the new analytic model, as per Ref. 32. This model is based on the following representation of the shock velocity U_s as a function of the particle velocity U_p over the three U_p intervals that is continuous and smooth from one interval to the next:

$$U_s = \begin{cases} C + BU_p + AU_p^2, & 0 \le U_p \le U_p^* = \dfrac{2(c-C)}{B-b}, \\ c + bU_p + aU_p^2, & U_p^* \le U_p \le U_p^{**} = nU_p^*, \\ -\dfrac{d}{f} + \dfrac{4}{3}U_p + \dfrac{dU_p}{1+fU_p}, & U_p \ge U_p^{**}. \end{cases} \tag{1}$$

The corresponding expressions for P along the principal Hugoniot are

$$P = \begin{cases} \dfrac{4\rho_0 C^2 \eta(\eta-1)}{\left\{\eta - B(\eta-1) + \sqrt{[\eta - B(\eta-1)]^2 - 4AC(\eta-1)^2}\right\}^2}, & 0 \le U_p \le U_p^*, \\ \dfrac{4\rho_0 c^2 \eta(\eta-1)}{\left\{\eta - b(\eta-1) + \sqrt{[\eta - b(\eta-1)]^2 - 4ac(\eta-1)^2}\right\}^2}, & U_p^* \le U_p \le U_p^{\max} = \sqrt{\dfrac{c}{a}}, \\ \dfrac{4\rho_0 c^2 \eta(\eta-1)}{\left\{\eta - b(\eta-1) - \sqrt{[\eta - b(\eta-1)]^2 - 4ac(\eta-1)^2}\right\}^2}, & U_p^{\max} \le U_p \le U_p^{**}, \\ \dfrac{\rho_0}{4f^2}\dfrac{\eta}{\eta-1}\left(\sqrt{12d\dfrac{\eta-1}{\eta-4}+1}-1\right)^2, & U_p \ge U_p^{**}, \end{cases} \tag{2}$$

which define the pressure along the Hugoniot as a continuous and smooth function of compression ratio $\eta \equiv \rho/\rho_0$, where ρ is the density and the subscript 0 indicates the initial (unshocked) state.

In the above formulas, $0 \le U_p \le U_p^*$ corresponds to the low-P regime, and $U_p^{\max} \le U_p \le U_p^{**}$ and $U_p \ge U_p^{**}$ to the med-P and high-P regimes, respectively. The value of U_p^{**} is found from the equation[32]

$$\left[c + \left(b - \frac{4}{3}\right)U_p^{**} + aU_p^{**2}\right]^2 = L\left(b - \frac{4}{3} + 2aU_p^{**}\right). \tag{3}$$

Here, $L \equiv \frac{2}{3}E$, where $E = E_{\rm coh} + E_{\rm dis} + E_{\rm ion}$ is the sum of cohesive, dissociation and ionization energies in going from ambient T to $T \to \infty$.[32] Thus, $L = \frac{2}{3}E \approx \frac{2}{3}E_{\rm ion}$, since $E_{\rm ion} \gg E_{\rm coh}$ and $E_{\rm ion} \gg E_{\rm dis}$. Following Ref. 38, we adopt $E_{\rm ion} \approx 13.6Z^{2.4}$ eV/atom. We tested this formula against the experimental total ionization energies from Ref. 39 for $1 \le Z \le 29$ (Cu), and the experimental and (or) theoretical ones from Ref. 40 for the remaining Z up to $Z = 118$ (oganesson, Og). We determined that the average root-mean-square deviation of the values it predicts from the corresponding experimental and/or theoretical values across the periodic table is less than 2%. The

TABLE I. Numerical values of the parameters for the analytic model of the principal Hugoniot for the two Hugoniot standards Cu and Ag and the two shock-ramp pusher standards Ir and Pt.

	Z	ρ_0 (g/cm^3)	C (km/s)	B	$A\times10^2$ [(km/s)$^{-1}$]	c (km/s)	b	$a\times10^5$ [(km/s)$^{-1}$]	L [(km/s)^2]	d	$f\times10^3$ [(km/s)$^{-1}$]	U_p^* (km/s)	$U_p^{\max}$ (km/s)	U_p^{**} (km/s)
Cu	29	8.93	3.916	1.511	−0.792 967	7.122 46	1.190 06	10.118 8	44 885.5	0.883 324	4.436 16	19.981 7	265.308	887.140
Ag	47	10.49	3.242	1.564	−1.581 93	5.555 33	1.180 44	7.969 30	84 067.7	5.209 64	7.872 07	12.062 4	264.025	1241.07
Ir	77	22.56	3.884	1.635	−2.545 91	5.939 09	1.176 98	6.077 85	155 527	7.347 45	6.873 30	8.973 80	312.597	1673.11
Pt	78	21.45	3.627	1.533	−1.541 17	5.685 52	1.176 07	6.042 27	157 978	11.947 4	8.696 38	11.534 6	306.750	1698.75

largest deviation, ~9%, is for He. Since one mole corresponds to A gram, where A is the atomic mass, we have

$$L \approx 9.07Z^{2.4}\frac{\text{eV}}{\text{atom}} \approx 875Z^{2.4}\frac{\text{kJ}}{\text{mol}} = 875\frac{Z^{2.4}}{A}\left(\frac{\text{km}}{\text{s}}\right)^2.$$

Taking into account that $A/Z \approx 2 + 0.006Z$ (which is very accurate for $Z \gtrsim 6$[41]), and hence $A \approx 2Z + 0.006Z^2$, this reduces to

$$L \approx \frac{875Z^{2.4}}{2Z + 0.006Z^2}\left(\frac{\text{km}}{\text{s}}\right)^2. \tag{4}$$

In the above formulas for P, $U_p^* \le U_p \le U_p^{\max}$ and $U_p^{\max} \le U_p \le U_p^{**}$ correspond to the two sub-regimes of the med-P regime, namely, those below and above the turnaround point of $U_p^{\max} = \sqrt{c/a}$.[32] Theoretical calculations show that in the 100–500 Mbar range, the U_s–U_p dependence is also nearly linear, with a slope whose value is basically universal for all of the substances, ~1.2; see Fig. 2 of Ref. 38, Fig. 2 of Ref. 42, Fig. 2(a) of Ref. 43, and Fig. 10.2 of Ref. 44. The physical reasons for this behavior of $U_s = U_s(U_p)$ are analyzed in detail by Johnson[36,37] and Nellis and co-workers.[43,44] Johnson[45] also explains why, as U_p goes up, the compression ratio reaches its maximum, $\eta_{\max}$, such that $4 < \eta_{\max} < 7$, and then starts decreasing with increasing U_p and asymptotes to 4 as $U_p \to \infty$, in agreement with the physics of an ideal gas. The point of maximum compression is referred to as a turnaround point, since at this point the $\eta = \eta(U_p)$ behavior changes from increasing with U_p to decreasing with U_p. It corresponds to $P_{\max} \equiv P(\eta_{\max}) \sim 1$–$10$ Gbar, as mentioned above (typically, $P_{\max}$ increases with Z). A simple linear U_s–U_p dependence cannot capture this behavior of η, and therefore, to adequately describe the shock Hugoniot at $P \sim P_{\max}$, in a series of papers Kalitkin and co-workers[35,42,46,47] have advocated the idea that the results of the quantum-statistical model can be very reliably represented by a parabolic U_s–U_p relation

$$U_s = c + bU_p + aU_p^2, \qquad c, b > 0, \quad 0 < a \ll 1, \tag{5}$$

and a small quadratic term ($a \sim 10^{-4}$ s/km) is all that is needed to model a turnaround point. The use of (5) in the Rankine–Hugoniot relations leads to

$$\eta_{\max} = 1 + \frac{1}{b + 2\sqrt{ac} - 1},$$
$$U_p^{\max} \equiv U_p(\eta_{\max}) = \sqrt{\frac{c}{a}}, \tag{6}$$
$$U_s^{\max} \equiv U_s(\eta_{\max}) = 2c + b\sqrt{\frac{c}{a}}$$

and

$$P(\eta_{\max}) = \rho_0 U_s(\eta_{\max})U_p(\eta_{\max}) = \rho_0\frac{c}{a}\left(b + 2\sqrt{ac}\right).$$

In the high-P regime (past the turnaround point) described by the last lines of (1) and (2), corresponding to $U_p \ge U_p^{**}$, the system approaches the ideal gas limit,[32] and $\eta \to 4$ from the right, as in Figs. 1–4. The numerical values of the coefficients f and d in these lines are given by the formulas[32]

$$f = \frac{a\left[(4-3b)\sqrt{\frac{c}{a}}n - 3c(1+n^2)\right]}{3a\left[L + c\sqrt{\frac{c}{a}}n(1+n^2)\right] - c(4-3b)n^2},$$
$$d = L\left\{\frac{a\left[(4-3b)\sqrt{\frac{c}{a}}n - 3c(1+n^2)\right]}{3a\left[L + c\sqrt{\frac{c}{a}}n(1+n^2)\right] - c(4-3b)n^2}\right\}^2, \tag{7}$$

with $n = U_p^{**}/U_p^{\max}$, U_p^{**} being the (only positive) solution of (3). For a given Z, these coefficients are functions of the parameters c, b, and a only, which are themselves functions of Z only. In this respect, the construction of the complete principal Hugoniot for any material does not require any additional parameter except the experimental low-P values of C and B or, equivalently, ρ_0 and the

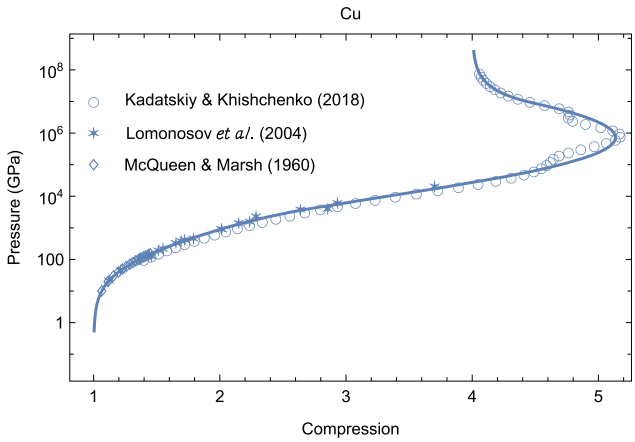

FIG. 1. Principal Hugoniot of Cu as P vs η ("Compression"): our new analytic model (solid line) vs the experimental data from Refs. 3, 21, and 51, and the theoretical calculations in Refs. 52 and 53 using the average-atom approximation implemented with three quantum-statistical models, specifically Thomas–Fermi, Thomas–Fermi with quantum and exchange corrections, and Hartree–Fock–Slater.

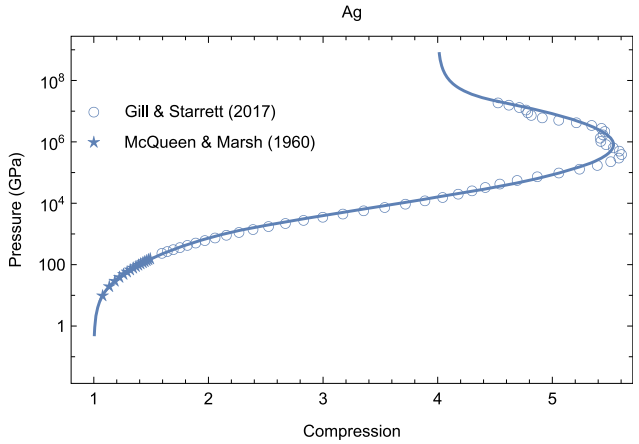

FIG. 2. Principal Hugoniot of Ag as P vs η ("Compression"): our new analytic model (solid line) vs the experimental data from Ref. 3 and the theoretical calculations in Ref. 54 using the relativistic Green's function quantum average atom code Tartarus.

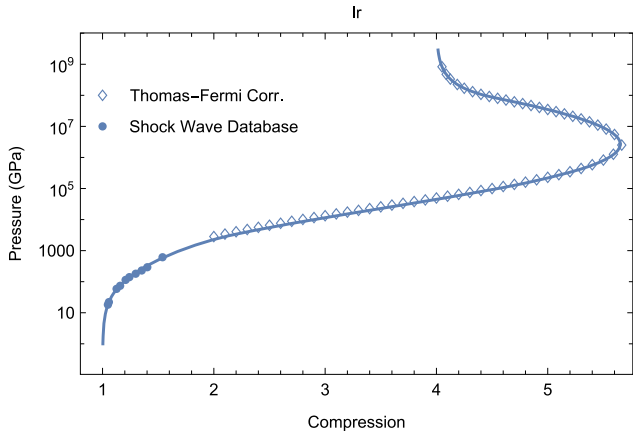

FIG. 3. Principal Hugoniot of Ir as P vs η ("Compression"): our new analytic model (solid line) vs the experimental data from Ref. 55 ("Shock Wave Database") and our own theoretical calculations, similar to those in Ref. 56 for Pt, using the Thomas–Fermi model with corrections ("Thomas–Fermi Corr.").

isentropic bulk modulus $\mathcal{B}_s$ and its pressure derivative $\mathcal{B}'_s$, in view of the relationships[36,37] $C = \sqrt{\mathcal{B}_s(\rho_0)/\rho_0}$ and $B = \frac{1}{4}[\mathcal{B}'_s(\rho_0) + 1]$.

The numerical values of all the parameters required for the construction of the principal Hugoniots of the two Hugoniot standards Cu and Ag, as well as the two shock-ramp pusher standards Ir and Pt, are listed in Table I. In each case, the values of C and B come from fitting $U_s = C + BU_p$ to the low-pressure shock-wave data of Refs. 3 and 48.

Note that our values of C, B, A, c, b, and a for Cu are consistent with those suggested by Kalitkin and Kuz'mina in Ref. 26: 3.9216, 1.5159, -0.821×10^{-2}, 7.1103, 1.190 36, and 10.021×10^{-5}, respectively. In Ref. 26, only two of the three pressure regimes of the principal Hugoniot were considered, namely, the low-P and med-P ones. Our values of C and B for Cu are consistent with those

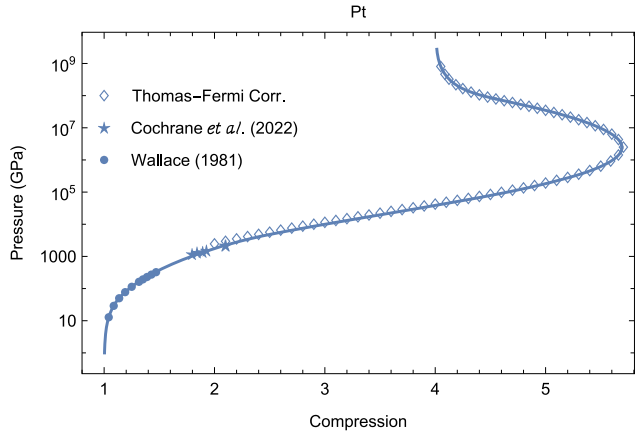

FIG. 4. Principal Hugoniot of Pt as P vs η ("Compression"): our new analytic model (solid line) vs the experimental data from Refs. 57 and 58 and the theoretical calculations in Ref. 56 using the Thomas–Fermi model with corrections ("Thomas–Fermi Corr.").

coming from the most recent experimental shock-wave data on Cu in Refs. 49 and 50: $C = 3.91$, $B = 1.51$, and $C = 3.909 \pm 0.007$, $B = 1.505 \pm 0.004$, respectively. The complete low-P-regime parameter set (C, B, A) is consistent with that of Ref. 24, $(3.899, 1.52, -0.009)$, from interpolation of the low-P experimental and high-P theoretical data, which is analogous to our interpolation between the low-P and med-P regimes through the addition of an extra AU_p^2 term to $U_s = U_s(U_p)$ for the former.

Figures 1–4 compare the new model with the four sets of experimental and independent theoretical data on Cu, Ag, Ir, and Pt, respectively. As can be clearly seen, in each of the four cases, agreement with the data is excellent.

A. Limit of the validity of the formula (5)

Kalitkin and Kuzmina[33,34] assumed that the parabolic form (5) is valid up to $U_p \sim 2U_p^{\max}$. This assumption is based on a purely empirical observation that a transition to the $\eta \to 4$ asymptotic regime must occur at (much) higher U_p, and so it must be safe to use (5) up to $U_p \sim 2U_p^{\max}$. Our results on the four shock standards demonstrate that the value of $U_p^{**}/U_p^{\max}$ ranges from ~3.3 for Cu to ~5.5 for Pt, i.e., that it is larger than 2. In fact, it can be as large as ~10 (Fig. 5 of Ref. 32). Let us dwell on this point in some more detail.

The upper branch of $P(\eta)$ beyond the turnaround point [the third line of (2)] asymptotes to the value of η at which its denominator turns zero. It is apparent that this value is 1. Hence, $P(\eta)$ across the turnaround point, as a combination of both lower [second line of (2)] and upper branches, although it correctly reproduces the turnaround feature of the Hugoniot, exhibits the unphysical behavior $\eta \to 1$ instead of the correct $\eta \to 4$ limit as $U_p \to \infty$. In this subsection, we will estimate the limiting value of U_p beyond which the analytic form of the upper branch of $P(\eta)$ is no longer valid. That is, at U_ps higher than some $U_p^{\lim}$, the system leaves the med-P regime and enters the high-P regime described by the last lines of (1) and (2).

To determine $U_p^{\lim}$, the limiting value of U_p mentioned above, we first calculate the η that corresponds to $U_p = nU_p(\eta_{\max}) = n\sqrt{c/a}$. It follows from (5) and one of the Rankine–Hugoniot relations, namely, $\eta = U_s/(U_s - U_p)$,[32] that

$$\eta\left(n\sqrt{c/a}\right) = 1 + \frac{1}{b + (n + 1/n)\sqrt{ac} - 1}. \tag{8}$$

With $n > 0$ and $n \neq 1$, $n + 1/n > 2$, and hence $\eta(n\sqrt{c/a}) \leq \eta_{\max}$ at all $n > 0$, i.e., $U_p = \sqrt{c/a}$ does correspond to a maximum compression ratio. Note that $\eta = 1$ at $n = 0$ ($U_p = 0$), and $\eta \to 1$ as $n \to \infty$, i.e., η does asymptote to 1 as $U_p \to \infty$, as mentioned above. Now, to determine the value of $U_p^{\lim}$, we make the single assumption that the transition from the med-P regime to the next high-P one occurs at some $\eta(n\sqrt{c/a}) > 4$; in other words, in the high-P regime, the system approaches its limiting compression ratio value of 4 from the right, i.e., η remains larger than 4 at all $U_p \geq U_p(\eta_{\max})$. It then follows from the above formula that $\eta(n\sqrt{c/a}) > 4$ provided that

$$n + \frac{1}{n} < \frac{\frac{4}{3} - b}{\sqrt{ac}}, \tag{9}$$

from which N, the limiting value of n for the validity of (9), is found.

Let us first obtain the lower bound on $(\frac{4}{3} - b)/\sqrt{ac}$. Since $\eta_{\max} > 4$, it follows from (6) that $b + 2\sqrt{ac} < \frac{4}{3}$, or $\frac{4}{3} - b > 2\sqrt{ac}$, and therefore

$$\frac{\frac{4}{3} - b}{\sqrt{ac}} > 2, \tag{10}$$

supporting the assumption of Kalitkin and Kuzmina. In reality, however, $5 \lesssim (\frac{4}{3} - b)/\sqrt{ac} \lesssim 15$, except for low-$Z$ ($Z \lesssim 10$) (see Fig. 5), and so we can put $(\frac{4}{3} - b)/\sqrt{ac} \gg 1$. Then the solution of the inequality (9) is

$$n < N \approx \frac{\frac{4}{3} - b}{\sqrt{ac}} - \frac{\sqrt{ac}}{\frac{4}{3} - b}. \tag{11}$$

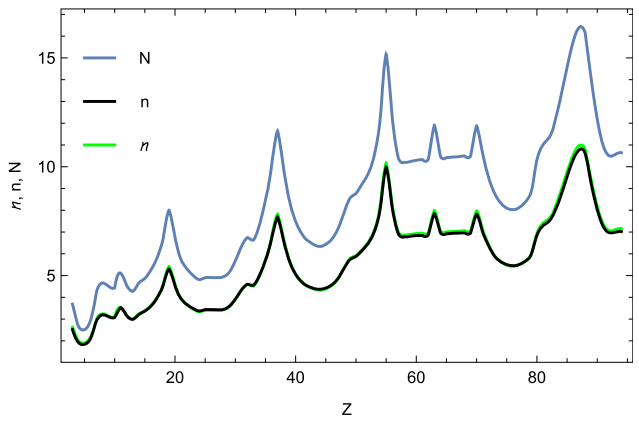

FIG. 5. Comparison between N in (11), ν in (12), and $n \equiv U_p^{**}/\sqrt{c/a}$, where U_p^{**} is the solution of (3), all three being functions of Z.

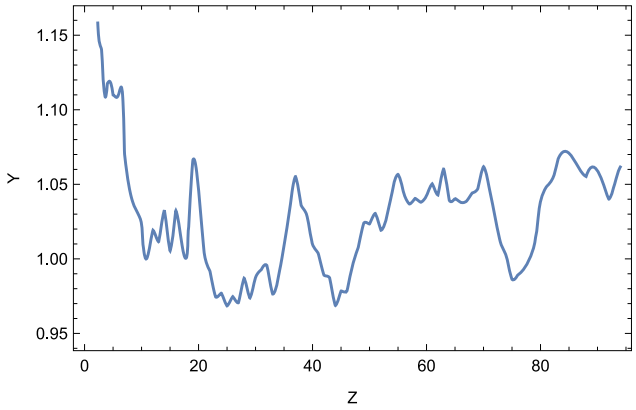

FIG. 6. Y defined in (23) as a function of Z.

In practice, the (approximate) relation $N = (\frac{4}{3} - b)\sqrt{ac}$ can be used, which is very accurate and agrees with Kalitkin and Kuzmina, since $N > 2$.

Finally, we note that the exact transition point between the med-P and high-P regimes as the solution of (3) can be approximated very accurately by the formula

$$U_p^{**} \approx \nu U_p^{\max}, \qquad \nu \equiv \frac{2}{3}\frac{\frac{4}{3} - b}{\sqrt{ac}} \approx \frac{2}{3}N, \tag{12}$$

that is,

$$U_p^{**} \approx \frac{2}{3}\frac{\frac{4}{3} - b}{a}. \tag{13}$$

The values of N, ν, and $n \equiv U_p^{**}/\sqrt{c/a}$, where U_p^{**} is the solution of (3), are compared with each other as functions of Z in Fig. 5. It can clearly be seen that ν is a very good approximation for n; in fact, the relative error does not exceed a few percent for all Z.

Using ν defined by (12) as n in (7) leads to the approximate relations

$$f = \frac{9a[2(4 - 3b)^2 - 81ac]}{729a^2L + 162ac(4 - 3b) - 4(4 - 3b)^3}, \qquad d = Lf^2. \tag{14}$$

The use of U_p^{**} from (13) in (3) leads, via $c \ll (b - \frac{4}{3})U_p^*$ and $c \ll aU_p^{*2}$, to the (approximate) formula

$$Y \equiv \frac{2}{27}\frac{(4 - 3b)^{3/2}}{aL^{1/2}} = 1. \tag{15}$$

Figure 6 shows Y as a function of Z and demonstrates that for $Z \gtrsim 10$, $Y \approx 1.02 \pm 0.05$, and so (15) is indeed quite accurate.

It follows from (15) that $a \simeq \frac{2}{27}(4 - 3b)^{3/2}/L^{1/2}$. The use of $b(Z) \approx \text{const} = 1.18$ in this formula (see Table I: the average of the four values of b is 1.181) leads to $a \approx 0.023/L^{0.5}$, which establishes the physical meaning of the parameter a of the TFK model as being directly related to the total ionization energy. The above formula is quite accurate as well: the four values of $a \times 10^5$ to be compared with the corresponding values in Table I are 10.86, 7.933, 5.832, and 5.787.

Using the above relation between a, b, and L leads to more simplified analogs of (7): $f = [2(4-3b)^2 - 81ac]/[18c(4-3b)]$ and $d = (4-3b)[2(4-3b)^2/(243ac) - \frac{1}{3}]^2$. The use of $b = 1.18$ can simplify these formulas even further.

B. Grüneisen parameter along the principal Hugoniot

Pressures in excess of ~30 TPa can be achieved in laser-driven shock impedance matching experiments using the Cu (or Ag) standard.[59–61] In such experiments, (precise) knowledge of the release isentropes (adiabats) is needed. Indeed, if the shock impedance of Cu (or Ag) is higher than that of most of the sample materials, which is expected to be the case, then the adiabatic release description is more important for reducing the experimental data uncertainties than the standard Hugoniot itself. Then, (precise) knowledge of the Grüneisen parameter becomes necessary; for example, the temperature along the adiabat is given by $T(\rho) = T(\rho_{\rm ref}) \exp\left\{\int_{\rho_{\rm ref}}^{\rho} [\gamma(r)/r] dr\right\}$, where $\gamma(r)$ is the Grüneisen parameter, which is assumed to be a function of density only, and $\rho_{\rm ref}$ is some reference density [to which $T(\rho_{\rm ref})$ corresponds]. In this subsection, we suggest a way to calculate the Grüneisen parameter along the principal Hugoniot in our analytic model. We choose Cu as the prototype for this calculation.

Johnson[36–38] derived the exact relation

$$\frac{\mathcal{B}_s}{P} - \frac{\mathcal{C}}{U_p} = 3\mathcal{S} - 1 + \mathcal{S}(2\mathcal{S} - 2 - \gamma)\frac{U_p}{\mathcal{C}}, \tag{16}$$

where $\gamma \equiv \frac{1}{\rho}\frac{\partial p}{\partial E}|_\rho$ is the Grüneisen parameter, $\mathcal{S}$ the (instantaneous) slope of the tangent line of the U_s–U_p curve, and $\mathcal{C}$ the $U_p = 0$ intercept of the tangent line (in other words, $U_s = \mathcal{C} + \mathcal{S}U_p$). All the quantities in (16), including γ, are on the Hugoniot and thus are functions of a Hugoniot variable, such as U_p, that we chose for the new analytic model. In Ref. 38, Johnson claimed that "For small U_p, $\mathcal{B}_s/P$ diverges as $1/U_p$, but, as U_p increases, $\mathcal{B}_s/P$ decreases to $\gamma + 1$" and remains there for $U_p \gtrsim 10$ km/s and well above the turnaround point. In other words, $\mathcal{B}_s/P \approx \gamma + 1$ in the entire med-P regime, and perhaps in the high-P regime, too. We can easily check whether the latter is the case. Taking into account that the approach to the ideal gas regime should agree with the large-U_p expansion of $U_s(U_p)$ given by the last line of (1), under the assumption that Debye–Hückel theory[62] describes very high-temperature gas, for large U_p, $\gamma = \frac{2}{3} - \beta/U_p^3, \beta > 0$.[38] Then, the use in (14) of the corresponding asymptotic forms of $\mathcal{C}$ and $\mathcal{S}$ from Ref. 32 and $\beta = d/f^3$[32] gives $\mathcal{B}_s/P = \frac{5}{3} - \beta/U_p^3$, i.e., $\gamma + 1$. Thus, this relation holds in the high-P regime. Assuming its validity in the med-P regime, using $\gamma + 1$ on the left-hand side of (16), along with $\mathcal{C} = c - aU_p^2$ and $\mathcal{S} = b + 2aU_p$, and solving for γ gives

$$\gamma \equiv \gamma(U_p) = 2(b-1) + 3aU_p + \frac{c}{U_p}. \tag{17}$$

At the turnaround point, $\gamma(U_p^{\rm max}) \equiv \gamma_{\rm max} = 2(b-1) + 4\sqrt{ac}$, which is equal to $2/(\eta_{\rm max} - 1)$, in agreement with Jonhson's[38] constraint on γ that $\gamma = 2/(\eta - 1)$ at every point on the Hugoniot where $\mathcal{C} = 0$, such as the turnaround point, or the $U_p \to \infty$ limit in which $\eta = 4$ and $\gamma = \frac{2}{3}$.

The Grüneisen gamma defined in (17) has a minimum, at $U_p = 1/\sqrt{3}\sqrt{c/a} = U_p^{\rm max}/\sqrt{3}$, and its value at this U_p is $2(b-1) + 2\sqrt{3}\sqrt{ac}$, slightly below $\gamma_{\rm max}$. As Fig. 6 clearly demonstrates, once U_p is greater than ~7 km/s or so, γ goes through a very broad minimum with very small variation in γ,[38] and in the area of this broad minimum, $\gamma \approx 0.4$[38] (for Cu, the actual value is ~0.45).

Now, γ in the low-P regime is modeled as[63]

$$\gamma(U_p) = \gamma_0 + g_1 U_p + g_2 U_p^2, \qquad g_1 < 0, \tag{18}$$

where γ_0 is the ambient Grüneisen parameter and g_1 and g_2 are given by formulas from Ref. 63. For Cu, we slightly modify the corresponding formulas to have the resulting γ continuous and smooth across the low-P–med-P transition point U_p^*:

$$g_1 = 3\left(a + \frac{c}{U_p^{*2}}\right) - 2\frac{\gamma_0 - 2(b-1)}{U_p^*}, \tag{19}$$

$$g_2 = \frac{\gamma_0 - 2(b-1)}{U_p^{*2}} - \frac{2c}{U_p^{*3}}. \tag{20}$$

Similarly, in the high-P regime, γ is modeled as

$$\gamma(U_p) = \frac{2}{3} - \frac{d/f^3}{U_p^3} + \frac{g_4}{U_p^4} + \frac{g_5}{U_p^5}. \tag{21}$$

The values of g_4 and g_5 are then determined by imposing the continuity and smoothness of γ across the med-P–high-P transition point U_p^{**}:

$$g_4 = \frac{2d}{f^3}U_p^{**} + 4cU_p^{**3} + 10\left(b - \frac{4}{3}\right)U_p^{**4} + 18aU_p^{**5}, \tag{22}$$

$$g_5 = -\left[\frac{d}{f^3}U_p^{**2} + 3cU_p^{**4} + 8\left(b - \frac{4}{3}\right)U_p^{**5} + 15aU_p^{**6}\right]. \tag{23}$$

Finally, to obtain the Grüneisen parameter as a function of η, we use the formulas for $U_p = U_p(\eta)$ from Ref. 32 in each of the three P regimes. The entire Grüneisen gamma for Cu along its principal

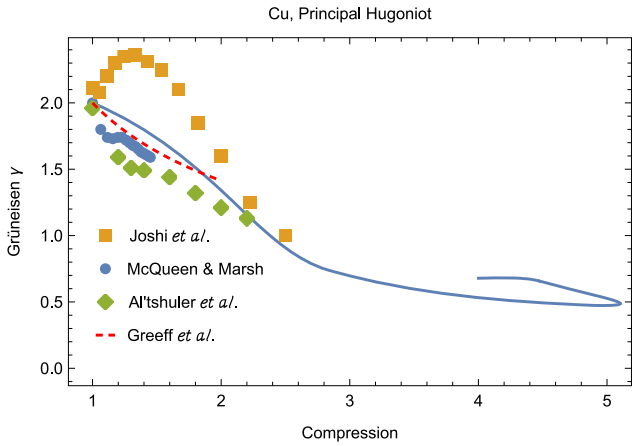

FIG. 7. Grüneisen gamma for Cu along its principal Hugoniot vs η ("Compression"): our new analytic model (solid line) vs the theoretical results of Ref. 64, the results of Refs. 3 and 65 using some functional forms of $\gamma(\rho)$ applied to the corresponding experimental data, and the theoretical model of Ref. 66.

Hugoniot, as a combination of those in the corresponding P regimes, given by (17), (18), and (21), is shown in Fig. 7.

Of course, our approach to calculate the Grüneisen parameter along the Hugoniot requires further detailed analysis of the assumptions made here, for their validation, as well as more examples of real cases such as that of Cu considered in this work. We will present a more detailed study of the Grüneisen gamma along the Hugoniot in a subsequent publication.

III. CONCLUDING REMARKS

The following is a brief summary of the findings of this work. We have presented the principal Hugoniots of four shock standards, namely, two Hugoniot standards Cu and Ag and two pusher standards Ir and Pt for modified shock-ramp experiments, using the analytic framework established in our previous publication.[32] All four sets of relevant parameters are summarized in Table I.

We have established a theoretical limit for the validity of the parabolic representation (5) for the TFK model, namely, (11), and its practical implementation in terms of the formulas (12) and (13), which very closely approximate, respectively, the exact values of $n = U_p^{**}/U_p^{\max}$ and U_p^{**} as the solution of (3).

Let us note that in a more realistic case of a shock compression of a substance beyond the corresponding turnaround point, the Hugoniot must be modeled taking into account the well-known effects of the contributions of both the equilibrium radiation of hot plasma and relativistic effects.[52,67–69] Indeed, at a turnaround point, $U_p \sim 300$ km/s (see Table I), which constitutes 0.1% of the speed of light, and at the med-P–high-P transition point, $U_p \sim 1700$ km/s, which is about 0.5% of the speed of light. Hence, as the system enters the high-P regime, relativistic effects are expected to start manifesting themselves and eventually to dominate the evolution of the system at even higher U_p. Our model can in principle be modified to incorporate these effects. For instance, the radiation-dominated (the so-called strong shock) regime can be taken into account by replacing the equations for $U_s(U_p)$ and $P(\eta)$ describing the high-P regime with their counterparts stemming from the physics of a photon gas. This goes beyond the scope of the present work, but will be undertaken in a subsequent study.

We also note that the new model discussed in this work does not incorporate potential electronic shell effects in our med-P and high-P regimes. If present, they manifest themselves in terms of some irregularities of $P = P(\eta)$ over some (small) regions of P; such irregularities are seen, for example, in Fig. 1 in the theoretical data on Cu around 10^6 GPa from Refs. 52 and 53 and in Fig. 2 in the theoretical model for Ag around $\sim 10^{5.5}$–$10^{6.5}$ GPa from Ref. 54. Such effects cannot be predicted by the new model, but, if firmly established, they can be added to the model by considering additional region(s) of P described by the corresponding $U_s = U_s(U_p)$ functional forms. We plan to undertake such an addition of electronic shell effects to the new model in a subsequent study.

Our new analytic model of the principal Hugoniot[32] can be used for the validation of the P–V–T EOS, by comparing the Hugoniot produced by the EOS with that given by the model. Also, the new model itself can be used as a basis for EOS construction. Indeed, if the Grüneisen parameter along the Hugoniot is available from, for example, the approach discussed in this work, then it can be used in the Mie–Grüneisen-type EOS $P - P_{\rm H} = \gamma_{\rm H}\rho(E - E_{\rm H})$,[70] where the subscript "H" indicates that the corresponding variable is that under shock-compression conditions. This EOS can then be brought into direct correspondence to the more familiar Mie–Grüneisen (M–G) EOS $P - P_c = \gamma\rho(E - E_c)$, where the subscript c indicates cold $(T = 0)$ conditions, since there exists a direct algebraic connection between $\gamma_{\rm H}$ (of this work) and γ of the M–G EOS.[70] In this way, the Cu Hugoniot standard can be directly related to the Cu EOS standard,[66] the reliability of which is critical for the ruby pressure scale, as discussed in Sec. I.

The analytic model developed in our previous study[32] and applied to four shock standards in this work can be used to calculate the Hugoniots of other substances. In this context, analytic knowledge of the regimes of the Hugoniot past the turnaround point is very important. In a recent publication,[71] a team of astronomers reported a detailed study of a pair of shock waves produced by the collision of two clusters of galaxies that occurred roughly a billion years ago. The shocks that are associated with cluster mergers are known as radio relics, and they can be used to probe the properties of the intergalactic space within the cluster, known as the intracluster medium, as well as intracluster dynamics. The study focused on a particular cluster called Abell 3667, which contains at least 550 galaxies and which is still coming together. It was concluded that the shock waves are propagating through the cluster at velocities of ~1500 km/s, which are roughly four times larger than the velocities corresponding to turnaround points, $U_s^{\max} = 2c + b\sqrt{c/a} \approx b\sqrt{c/a} \sim 1.2\sqrt{10^5} \sim 400$ km/s (see Table I). Moreover, at such shock velocities, many elements, especially the low-Z ones, will be under conditions that are beyond the validity of Kalitkin's parabolic representation (5), i.e., they will be in the high-P regime considered in this work. Hence, to predict the properties of the intracluster medium and to describe intracluster dynamics, an analytic model of the principal Hugoniot in the high-P regime is a must. Once the analytic formulas describing the high-P regime are available [the last lines of both systems of Eqs. (1) and (2)], the basic mechanical and thermodynamic properties of a material under intergalactic shock, such as the bulk modulus, Grüneisen parameter, energy, and temperature, along the principal Hugoniot can be derived from the Rankine–Hugoniot relations and (16) using the new model and some additional assumptions on the Grüneisen gamma.

ACKNOWLEDGMENTS

This research was carried out under the auspices of the U.S. DOE/NNSA.

AUTHOR DECLARATIONS

Conflict of Interest

The authors have no conflicts to disclose.

Author Contributions

Leonid Burakovsky: Investigation (lead); Writing – original draft (lead); Writing – review & editing (equal). **Dean L. Preston**: Formal analysis (equal); Investigation (equal); Writing – review & editing

(equal). **Scott D. Ramsey**: Investigation (equal); Project administration (equal); Writing – review & editing (equal). **Charles E. Starrett**: Investigation (equal); Writing – review & editing (equal). **Roy S. Baty**: Investigation (equal); Project administration (equal); Writing – review & editing (equal).

DATA AVAILABILITY

The data that support the findings of this study are available from the corresponding author upon reasonable request.

REFERENCES

[1] J. W. Forbes, "Impedance matching technique," in *Shock Wave Compression of Condensed Matter*, Shock Wave and High Pressure Phenomena (Springer-Verlag, Berlin, Heidelberg, 2012), pp. 31–57.

[2] J. M. Walsh, M. H. Rice, R. G. McQueen, and F. L. Yarger, "Shock-wave compressions of twenty-seven metals. Equations of state of metals," Phys. Rev. **108**, 196 (1957).

[3] R. G. McQueen and S. P. Marsh, "Equation of state for nineteen metallic elements from shock-wave measurements to two megabars," J. Appl. Phys. **31**, 1253 (1960).

[4] L. V. Al'tshuler, K. K. Krupnikov, B. N. Ledenev, V. I. Zhuchikhin, and M. I. Brazhnik, "Dynamic compressibility and equation of state of iron under high pressure," Sov. Phys. JETP **34**, 606 (1958).

[5] A. I. Funtikov, "Phase diagram and melting curve of iron obtained using the data of static and shock-wave measurements," High Temp. **41**, 850 (2003).

[6] J. M. Brown and R. G. McQueen, "Melting of iron under core conditions," Geophys. Res. Lett. **7**, 533, https://doi.org/10.1029/gl007i007p00533 (1980).

[7] J. M. Brown and R. G. McQueen, "Phase transitions, Grüneisen parameter, and elasticity for shocked iron between 77 GPa and 400 GPa," J. Geophys. Res. **91**, 7485, https://doi.org/10.1029/jb091ib07p07485 (1986).

[8] B. K. Godwal, F. González-Cataldo, A. K. Verma, L. Stixrude, and R. Jeanloz, "Stability of iron crystal structures at 0.3–1.5 TPa," Earth Planet. Sci. Lett. **409**, 299 (2015).

[9] A. S. Vladimirov, N. P. Voloshin, V. N. Nogin, A. V. Petrovtsev, and V. A. Simonenko, "Shock compressibility of aluminum at $p \gtrsim 1$ Gbar," JETP Lett **39**, 82 (1984).

[10] D. N. Polsin *et al.*, "Measurement of body-centered-cubic aluminum at 475 GPa," Phys. Rev. Lett. **119**, 175702 (2017); Erratum **120**, 029902 (2018).

[11] Yu. B. Kudasov *et al.*, "Lattice dynamics and phase diagram of aluminum at high temperatures," J. Exp. Theor. Phys. **117**, 664 (2013).

[12] S. R. Baty, L. Burakovsky, and D. Errandonea, "*Ab initio* phase diagram of copper," Crystals **11**, 537 (2021).

[13] S. R. Baty, L. Burakovsky, and D. Errandonea, "*Ab initio* phase diagram of silver," J. Phys.: Condens. Matter **33**, 485901 (2021).

[14] J.-P. Davis, J. L. Brown, and C. T. Seagle, "Off-Hugoniot mechanical response of metal standards at the Z machine," SNL Preprint SAND2018-2465C, 2018.

[15] M. D. Knudson, "Megaamps, megagauss, and megabars: Using the Sandia Z Machine to perform extreme material dynamics experiments," AIP Conf. Proc. **1426**, 35 (2012).

[16] L. Burakovsky, S. P. Chen, D. L. Preston, and D. G. Sheppard, "Z methodology for phase diagram studies: Platinum and tantalum as examples," J. Phys.: Conf. Ser. **500**, 162001 (2014).

[17] L. Burakovsky *et al.*, "*Ab initio* phase diagram of iridium," Phys. Rev. B **94**, 094112 (2016).

[18] C. Seagle, B. Reinhart, S. Alexander, J. Brown, and J.-P. Davis, "Shock compression of iridium," SNL Preprint SAND2019-6863C, 2019.

[19] H. K. Mao, J. Xu, and P. M. Bell, "Calibration of the ruby pressure gauge to 800 kbar under quasi-hydrostatic conditions," J. Geophys. Res. **91**, 4673, https://doi.org/10.1029/jb091ib05p04673 (1986).

[20] W. J. Carter, S. P. Marsh, J. N. Fritz, and R. G. McQueen, *Accurate Characterization of the High-Pressure Environment*, NBS Special Publication Vol. 326 (National Bureau of Standards, 1971), p. 147.

[21] I. V. Lomonosov and S. V. Fortova, "Wide-range semiempirical equations of state of matter for numerical simulation on high-energy processes," High Temp. **55**, 585 (2017).

[22] M. K. Wallace, J. M. Winey, and Y. M. Gupta, "Shock compression of silver to 300 GPa: Wave profile measurements and melting transition," Phys. Rev. B **104**, 014101 (2021).

[23] C. A. McCoy, M. D. Knudson, and S. Root, "Absolute measurement of the Hugoniot and sound velocity of liquid copper at multimegabar pressures," Phys. Rev. B **96**, 174109 (2017).

[24] H. Liu *et al.*, "Validation for equation of state in wide regime: Copper as prototype," Matter Radiat. Extremes **1**, 123 (2016).

[25] M. Guinan and D. Steinberg, "A simple approach to extrapolating measured polycrystalline shear moduli to very high pressure," J. Phys. Chem. Solids **36**, 829 (1975).

[26] N. N. Kalitkin and L. V. Kuz'mina, "Copper as a shockwave standard," Dokl. Phys. **43**, 276 (1998).

[27] M. C. Marshall *et al.*, "Developing quartz and molybdenum as impedance-matching standards in the 100-Mbar regime," Phys. Rev. B **99**, 174101 (2019).

[28] D. G. Hicks *et al.*, "Shock compression of quartz in the high-pressure fluid regime," Phys. Plasmas **12**, 082702 (2005).

[29] M. D. Knudson and M. P. Desjarlais, "Shock compression of quartz to 1.6 TPa: Redefining a pressure standard," Phys. Rev. Lett. **103**, 225501 (2009).

[30] M. D. Knudson and M. P. Desjarlais, "Adiabatic release measurements in α-quartz between 300 and 1200 GPa: Characterization of α-quartz as a shock standard in the multimegabar regime," Phys. Rev. B **88**, 184107 (2013).

[31] S. Root, J. P. Townsend, and M. D. Knudson, "Shock compression of fused silica: An impedance matching standard," J. Appl. Phys. **126**, 165901 (2019).

[32] L. Burakovsky, D. L. Preston, S. D. Ramsey, and R. S. Baty, "Analytic model of principal Hugoniot at all pressures," J. Appl. Phys. **132**, 215109 (2022).

[33] N. N. Kalitkin and L. V. Kuzmina, "Quantum-statistical Hugoniots of porous substances," Mat. Model. **10**(7), 111 (1998).

[34] N. N. Kalitkin and L. V. Kuzmina, "Wide-range characteristic thermodynamic curves," in *High-Pressure Shock Compression of Solids VII: Shock Waves and Extreme States of Matter*, edited by V. E. Fortov, L. V. Al'tshuler, R. F. Trunin, and A. I. Funtikov (Springer-Verlag, New York, 2004), p. 116.

[35] N. N. Kalitkin and L. V. Kuzmina, "Shock Hugoniots of 83 substances," Chem. Phys. Rep. **18**, 1913 (2000).

[36] J. D. Johnson, "General features of Hugoniots," LANL Preprint LA-13137-MS, 1996.

[37] J. D. Johnson, "General features of Hugoniots—II," LANL Preprint LA-13217-MS, 1997.

[38] J. D. Johnson, "The features of the principal Hugoniot," AIP Conf. Proc. **429**, 27 (1998).

[39] See https://en.wikipedia.org/wiki/Ionization_energies_of_the_elements_(data_page) for the experimental values of total ionization energies of elements with $1 \leq Z \leq 29$.

[40] R. W. Gómez, "A simple model to calculate total and ionization energies of any atom," Eur. J. Phys. **40**, 015403 (2019).

[41] See https://pages.uoregon.edu/epmalab/UCB_EPMA/Physically.htm for the plot of A/Z as a function of Z for the entire periodic table.

[42] L. V. Al'tshuler, N. N. Kalitkin, L. V. Kuz'mina, and B. S. Chekin, "Shock adiabats for ultrahigh pressures," Sov. Phys. JETP **45**, 167 (1977).

[43] N. Ozaki, W. J. Nellis, T. Mashimo *et al.*, "Dynamic compression of dense oxide ($Gd_3Ga_5O_{12}$) from 0.4 to 2.6 TPa: Universal Hugoniot of fluid metals," Sci. Rep. **6**, 26000 (2016).

[44] W. J. Nellis, "Warm dense matter at shock pressures up to 20 TPa (200 Mbar)," in *Ultracondensed Matter by Dynamic Compression* (Cambridge University Press, Cambridge, UK, 2017), pp. 130–138.

[45] J. D. Johnson, "Bound and estimate for the maximum compression of single shocks," Phys. Rev. E **59**, 3727 (1999).

[46] N. N. Kalitkin, L. V. Kuzmina, and A. I. Funtikov, "The main Hugoniots of 10 metals," Mat. Model. **14**(10), 27 (2002).

[47] E. S. Ivanchenko, N. N. Kalitkin, and L. V. Kuz'mina, "Main Hugoniot adiabats in the tefis database of thermophysical properties of substances (TEFIS)," Math. Models Comput. Simul. **1**, 383 (2009).

[48] *LASL Shock Hugoniot Data*, edited by S. P. Marsh (University of California Press, Berkeley; Los Angeles; London, 1980).
[49] S. A. Thomas, R. S. Hixson, M. C. Hawkins, and O. T. Strand, "Wave speeds in single-crystal and polycrystalline copper," Int. J. Impact Eng. **139**, 103506 (2020).
[50] M. Sims *et al.*, "Experimental and theoretical examination of shock-compressed copper through the fcc to bcc to melt phase transitions," J. Appl. Phys. **132**, 075902 (2022).
[51] P. R. Levashov, K. V. Khishchenko, I. V. Lomonosov, and V. E. Fortov, "Database on shock-wave experiments and equations of state available via internet," AIP Conf. Proc. **706**, 87 (2004).
[52] M. A. Kadatskiy and K. V. Khishchenko, "Theoretical investigation of the shock compressibility of copper in the average-atom approximation," Phys. Plasmas **25**, 112701 (2018).
[53] M. A. Kadatskiy, "Quantum-statistical calculation of thermodynamic properties of simple substances and mixtures at high energy densities," Ph.D. thesis, Joint Institute for High Temperatures, Russian Academy of Sciences, Moscow, Russia, 2019.
[54] N. M. Gill and C. E. Starrett, "Tartarus: A relativistic Green's function quantum average atom code," High Energy Density Phys. **24**, 33–38 (2017).
[55] See http://www.ihed.ras.ru/rusbank/ for shock wave database with a free internet access.
[56] V. P. Kopyshev, *Equations of State Theory* (RFNC-VNIIEF, Sarov, 2009) (in Russian); see also A. F. Nikiforov, V. G. Novikov, and V. B. Uvarov, *Quantum-Statistical Models of Hot Dense Matter: Methods for Computation Opacity and Equation of State* (Birkhäuser, Basel, 2005).
[57] D. C. Wallace, "Nature of the process of overdriven shocks in metals," Phys. Rev. B **24**, 5607 (1981).
[58] K. R. Cochrane *et al.*, "Platinum equation of state to greater than two terapascals: Experimental data and analytical models," Phys. Rev. B **105**, 224109 (2022).
[59] L. R. Veeser, J. C. Solem, and A. J. Lieber, "Impedance-match experiments using laser-driven shock waves," Appl. Phys. Lett. **35**(10), 761 (1979).
[60] H. C. Pant *et al.*, "Laser driven shock wave experiments for equation of state studies at megabar pressures," J. Phys.: Condens. Matter **14**, 10787 (2002).
[61] S. Root *et al.*, "Argon equation of state data to 1 TPa: Shock compression experiments and simulations," Phys. Rev. B **106**, 174114 (2022).
[62] L. D. Landau and E. M. Lifshitz, *Statistical Physics* (Addison-Wesley Publishing Company, Reading, PA, 1969).
[63] K. Nagayama and Y. Mori, "Simple method of calculating Grüneisen parameter based on the shock Hugoniot data for solids," J. Phys. Soc. Jpn. **63**, 4070 (1994).
[64] R. H. Joshi *et al.*, "Grüneisen parameter and equations of states for copper—High pressure study," Comput. Condens. Matter **15**, 79 (2018).
[65] L. V. Al'tshuler, S. E. Brusnikin, and E. A. Kuz'menkov, "Isotherms and Grüneisen functions for 25 metals," J. Appl. Mech. Tech. Phys. **28**, 129 (1987).
[66] C. W. Greeff, J. C. Boettger, M. J. Graf, and J. D. Johnson, "Theoretical investigation of the Cu EOS standard," J. Phys. Chem. Solids **67**, 2033 (2006).
[67] N. Yu. Orlov, M. A. Kadatskiy, O. B. Denisov, and K. V. Khishchenko, "Application of quantum-statistical methods to studies of thermodynamic and radiative processes in hot dense plasmas," Matter Radiat. Extremes **4**, 054403 (2019).
[68] M. A. Kadatskiy and K. V. Khishchenko, "Shock compressibility of iron calculated in the framework of quantum-statistical models with different ionic parts," J. Phys.: Conf. Ser. **774**, 012005 (2016).
[69] M. A. Kadatskiy and K. V. Khishchenko, "Comparison of Hugoniots calculated for aluminum in the framework of three quantum-statistical models," J. Phys.: Conf. Ser. **653**, 012079 (2015).
[70] S. D. Ramsey *et al.*, "Converging shock flows for a Mie-Grüneisen equation of state," Phys. Fluids **30**, 046101 (2018).
[71] F. de Gasperin *et al.*, "MeerKAT view of the diffuse radio sources in Abell 3667 and their interactions with the thermal plasma," Astron. Astrophys. **659**, A146 (2022).